Kinetic Simulations of Plasma Plume Potential in a Vacuum Chamber

IEPC-2013-343

Presented at the 33rd International Electric Propulsion Conference,
The George Washington University, Washington, D.C., USA
October 6–10, 2013

Joseph J. Wang,* Daoru Han,† and Yuan Hu‡
University of Southern California, Los Angeles, California, 90089, USA

Direct Simulation Monte Carlo and Particle-in-Cell simulations are carried out to study the potential of a mesothermal plasma plume in a vacuum chamber. The results show that the beam potential with respect to the ambient in a vacuum chamber is different from that in space because the facility plasma can prematurely terminate the plume expansion process. As a result, the plume potential measured in a vacuum chamber may be significantly lower than that under the in-space condition. This can lead to under estimation of the backflow of CEX ions and ionized contaminants in plasma thruster plume modeling.

I. Introduction

The potential of the plasma plume emitted from a plasma thruster is a critical parameter in electric propulsion. The plume potential is not only related to the beam emission and neutralization processes but also affects the thruster induced plasma and contamination environments ([1,2,3,4]). As few direct in-flight measurements currently exist, predictions of the plume potential are mostly based on ground measurements in vacuum chamber.

The plume emitted by an ion thruster type plasma source is composed of high-energy beam ions, thermal neutralizing electrons, un-ionized neutrals, and low-energy charge-exchange (CEX) ions generated by collisions between the beam ions and the neutrals in the plume. The characteristics of the beam ions and neutralizing electrons is that of a collisionless, mesothermal plasma flow with $v_{te} >> v_{beam} >> v_{ti}$, where v_{te}, v_{beam}, and v_{ti} are the electron thermal velocity, beam velocity, and ion thermal velocity, respectively. Plasma plumes emitted by other types of plasma thrusters often have a similar flow characteristics. For further discussions in this paper, we shall refer the beam ions and neutralizing electrons as the propellant plasma, the CEX plasma generated between beam ions and un-ionized neutrals from the thruster as the plume CEX plasma, and all other plasma populations in a vacuum chamber as the facility plasma. During vacuum chamber testing, a plasma thruster operates in an environment different from that in space. In particular, the facility plasma density in a vacuum chamber is typically a few orders of magnitude higher than the ambient plasma density in space.

Wang et al. showed that the potential of a collisionless, mesothermal plasma plume with respect to the ambient is controlled primarily by two processes.[5] The first is the electron-ion coupling inside the beam which determines beam neutralization, or the net charge inside the plume. The second is the plasma expansion outside the beam which connects the beam potential to that of the ambient. As the facility plasma and the boundary conditions imposed by the vacuum chamber wall can affect the plasma expansion process, ground measurements in a vacuum chamber may not accurately predict the in-space plume potential.

Few experimental or modeling studies have addressed the facility effects on plume potential predictions. Recently, Polansky et al.[6] measured the spatial distribution of the potential for a mesothermal Ar plasma

*Associate Professor, Department of Astronautical Engineering, josephjw@usc.edu
†Graduate Research Assistant, Department of Astronautical Engineering, daoruhan@usc.edu
‡Graduate Research Assistant, Department of Astronautical Engineering, yuanhu@usc.edu

plume (beam ion energy 1100 eV) emitted from a 4-cm diameter girded ion source in a vacuum chamber. The measurements showed that the plume expansion was terminated by the background plasma surrounding the beam.

Particle-in-Cell (PIC) simulation has become the standard approach in modeling plasma plumes. Simulation studies of plasma plumes typically fall into the following two groups. The majority of simulation studies (i.e. the first group) focused on the CEX plasma interactions *outside* the beam. These studies are based on using a hybrid PIC approach which models the CEX ions as macro-particles and and the electrons as a massless, equilibrium, isothermal fluid. A commonly used assumption is that the electron dynamics may be simplified by the Boltzmann relation $n_e = n_0 \exp((\Phi - \Phi_0)/T_e)$, where Φ_0 is the plume potential at thruster exit. In these models, the plume potential Φ_0 must be provided as an input input parameter. Hence, such simulation models only address CEX interactions at the ion time scale and are not capable of resolving the plume potential. The second group focused on the beam neutralization process *inside* the beam (see, for example,[7,8,9,10,11,12,13,14]). Using a full particle PIC approach, these studies considered the transient neutralization process. Due to computational limitations, such studies focused on idealized beam emission of only beam ions and neutralizing electrons in a vacuum at the electron time scale. The plasma beam potential was not addressed.

In order to obtain the plume potential self-consistently in a simulation, one must simultaneously resolve both the electron-ion coupling inside the beam and the plasma expansion outside the beam.[5] This requires one to adopt the fully kinetic approach and carry out a full particle PIC simulation of the entire transient process from the electron time scale to ion time scale associated with the establishment of the steady state plume potential. Moreover, a realistic ion to electron mass must be used in the simulation so the correct mesothermal velocity order ($v_{te} >> v_{beam} >> v_{ti}$) can be maintained.

Wang et al. carried out such a full particle PIC simulation for an idealized beam emission of only beam ions and neutralizing electrons in vacuum.[5] This paper extends Ref. 5 to further include both the facility plasma and the plume CEX plasma in the simulation model. The focus is to address the effects of the facility plasma on the plume potential in a vacuum chamber. The approach is based on the full particle Particle-in-Cell (PIC) and Direct Simulation Monte Carlo (DSMC) methods. Section II discusses the approach and simulation setup. Section III discusses the simulation results. A summary and conclusion are given in Section IV.

II. Simulation Model

II.A. Approach

We consider the emission of a mesothermal plasma plume into a background plasma. Let n_0, $n_{ambient}$, and $n_{chamber}$ denote the propellant plasma density at the thruster exit, the average ambient plasma density in space, and the average density of the facility plasma in a vacuum chamber, respectively. An ion thruster type plasma source also generates a plume CEX plasma in addition to the beam ions and neutralizing electrons. The CEX ion production in the plume is determined by the neutral plume density $n_{n,source}$, the beam ion density n_{beam}, the relative velocity between the beam ions and the neutrals v_{in}, and the CEX collision cross section σ_{cex},

$$\dot{n}_{cex,source}(\vec{x}) = n_{n,source}(\vec{x}) n_{beam}(\vec{x}) v_{in} \sigma_{cex} \tag{1}$$

The density of the neutral plume emitted by the thruster is given by

$$n_{n,source}(exit) = \frac{(1-\eta)\dot{m}}{m_i c_n A_o} \tag{2}$$

where η is the propellant utilization efficiency, $\dot{m}$ is the propellant mass flow rate, c_n the speed of neutrals, and A_o the total exit open area. For typical ion thrusters, orders of magnitude set apart the densities of the propellant plasma, the plume CEX plasma, and the ambient plasma, $n_0 >> n_{cex,source} >> n_{ambient}$.

When a plasma thruster operates in a vacuum chamber, its surrounding neutral environment is different from the neutral plume emitted from the thruster. Factors contributing to this difference include the reflections of the neutrals at chamber surface, neutralization of beam ions at chamber surface, and the gas pumping rate. Ionization of the background neutrals by the propellant plasma and secondary electron emissions at chamber wall lead to the generation of a facility plasma in the vacuum chamber. The facility plasma environment can be quite different from the ambient space plasma environment.

Obviously, the environment inside a vacuum chamber is highly dependent on the specific experiments considered. In this paper, we consider an experimental setup and vacuum chamber environment similar to that discussed in Ref. 6. In Ref. 6, the plasma source is a 4-cm diameter gridded ion source using Ar as propellant with a hot-filament neutralizer. The vacuum chamber is 0.915 m in diameter and 1.05 m in length. A detailed characterization of the vacuum chamber environment found that the facility plasma in Ref. 6 was generated primarily by CEX collisions between the beam ions and the neutral environment in the chamber. The contributions of the secondary electron emission at chamber wall was minimum as compared to the CEX plasma production.[15] Hence, in this study, we shall consider a facility plasma generated by CEX collisions with the background neutrals. Let $n_{n,chamber}$ denote the total neutral density inside a vacuum chamber. The CEX production rate for in-chamber operation is given by

$$\dot{n}_{cex,chamber}(\vec{x}) = n_{n,chamber}(\vec{x}) n_{beam}(\vec{x}) v_{in} \sigma_{cex} \tag{3}$$

We consider three different simulation cases in Sec. III. In all the cases, the plasma emission parameters are modeled after that in Ref. 6 and will be discussed in the next section. Case 1 simulates the in-space operation where we consider the emission of a plasma plume into an ambient space plasma of density $n_{ambient}$ in a simulation domain with open boundaries. Case 2 simulates the in-chamber operation where we consider the emission of a plasma plume into a vacuum chamber with a facility plasma. The in-chamber simulation models the experimental configuration of Ref. 6. Fig. 1 shows the experimental configuration with the relative dimensions of the vacuum chamber and thruster body in terms of the beam radius. The facility plasma density $n_{chamber}$ is estimated from Eq. (3). Case 3 also consider the in-chamber configuration shown in Fig. 1. However, in Case 3, we set the value of the facility plasma density $n_{chamber}$ to be the same as the $n_{ambient}$ used in Case 1 for comparison.

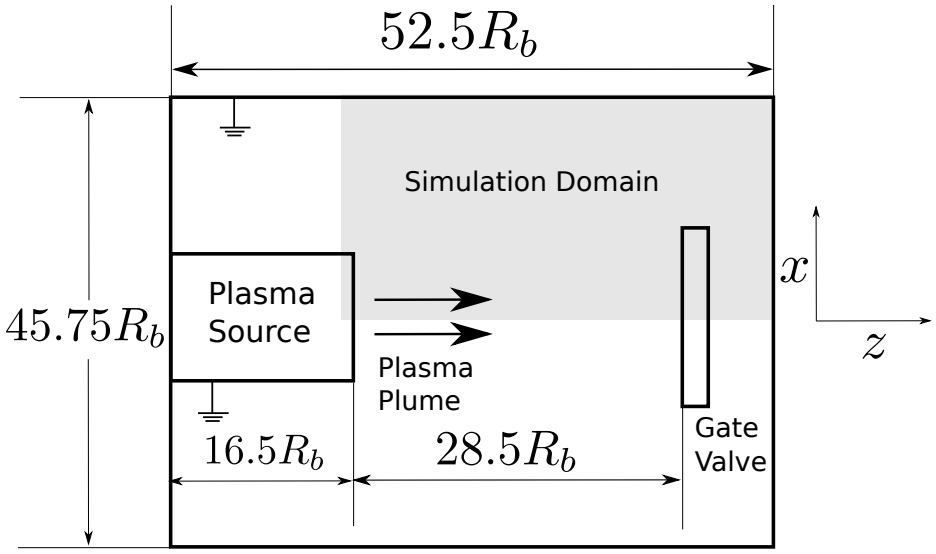

Figure 1. Plasma source testing schematics with the dimension shown in terms of the ion beam radius R_b

II.B. Direct Simulation Monte Carlo

In order to include the plume CEX ions and the facility plasma in the simulation, one needs to first obtain the neutral plume density, $n_{n,source}(\vec{x})$ and the total neutral density in the chamber, $n_{n,chamber}(\vec{x})$ respectively.

In this study, DSMC is applied to simulate the neutral molecules and obtain $n_{n,source}(\vec{x})$ and $n_{n,chamber}(\vec{x})$. The DSMC study directly models the plasma source and the experiments discussed in Ref. 6. The simulation domain is the entire vacuum chamber shown in Fig. 1.

The experimental operating condition considered is the same as that in Ref. 6, and is shown in Table 1. We consider a plasma source emission with a 4.1 sccm of argon gas flow rate. In the experiment, the pressure in the vacuum chamber during the plasma emission was maintained at $P_c \simeq 3.8 \times 10^{-6}$ Torr by a mechanical roughing pump and a cryogenic pump (pumping speed of 8,500 L/s). The current emitted and the neutral density at the source exit are also shown in Table 1. In the experiment, the plume CEX production rate is comparable to that of the NSTAR ion thruster.[6]

Table 1. Thruster operating conditions

I, mA	$\dot{m}$, sccm	η	$n_{n,exit}$, m^{-3}	P_c, Torr
10.	4.1	3.4%	2.9×10^{19}	3.8×10^{-6}

Table 2. plasma parameters at thruster exit.

	In Physical Unit	Normalized Value
n_{e0}	1.5×10^{15} m^{-3}	1.0
n_{i0}	4.9×10^{15} m^{-3}	3.26
T_{e0}	2 eV	1.0
λ_{D0}	0.4 mm	1.0
v_{beam}	72,809 m/s	0.122
v_{te}	594,918 m/s	1.0
v_{ti}	2201 m/s	0.0037

To obtain $n_{n,source}(\vec{x})$, macro-particles representing the un-ionized Ar were injected from the source exit into the simulation domain using a mixed inflow/wall condition. To obtain $n_{n,chamber}(\vec{x})$, macro-particles representing the high energy beam ion Ar^+ were also injected from the source exit for the purpose of generating the neutrals created at the gate valve and chamber wall. These macro-particles follow a line-of-sight trajectory until they hit the surface. They are then reflected as neutrals to join the DSMC calculation. Because the beam ions have an energy of 1100eV and thus their trajectories are not affected by the electric field in the chamber (on the order of a few Volts/m) in the chamber, such an approach is valid.

The velocities of Ar particles are sampled from a stationary Maxwellian distribution, and those of Ar^+ particles are sampled from a drifting Maxwellian distribution with a drifting velocity corresponding to the ion accelerating voltage. The temperature for the inflow particles is taken to be 500K. For in-chamber simulations, any Ar^+ ions impinging the chamber wall are reflected as Ar atoms under a fully-diffusive wall boundary condition. The chamber wall temperature is set to be 300K. Particles reaching the cryogenic pump surface are simply removed from the computational domain.

The DSMC simulation is carried out using an axi-symmetric code SUPGAS.[17] The code implements the standard DSMC method[16] using the variable hard sphere (VHS) model for inter-molecular collisions. The VHS model treats the gas as a collection of hard spheres whose total cross section σ_T can be expressed as a power-law function of relative speed g between the colliding particles:

$$\sigma_T \sim \sigma_{\text{ref}} g^{1-2\omega} \tag{4}$$

where $\sigma_{\text{ref}} = \pi d_{\text{ref}}^2$. Here, d_{ref} and σ_{ref} are the diameter and total cross section under a reference condition, respectively. The VHS model above leads to a power-law temperature dependence on viscosity,

$$\mu = \mu_{\text{ref}} \left(\frac{T}{T_{\text{ref}}} \right)^{\omega} \tag{5}$$

Following Ref. 16, we find $\mu_{\text{ref}} = 2.117 \times 10^{-5}$ kg/(m·s) at $T_{\text{ref}} = 273$ K, which lead to $d_{\text{ref}} = 4.17 \times 10^{-10}$ m, and $\omega = 0.81$ for argon.

II.C. Particle-in-Cell Simulation

PIC simulation is carried out to obtain the plasma plume potential. The PIC simulation code is a 3-dimensional (3D), full particle particle-in-cell (PIC) model extended from Ref. 5. The plasma species simulated by the PIC code include the beam ions and neutralizing electrons emitted from the source, the CEX ions generated in the plume, and the background (ambient or facility) ions and electrons. The electric field, particle trajectories, and the space charge are solved self-consistently from the Poisson's equation and Newton's second law subject to the required boundary conditions

$$\nabla \cdot (\epsilon_0 \vec{\nabla} \Phi) = e(n_e - n_i) \tag{6}$$

$$\frac{d}{dt}(m\vec{v}) = q\vec{E},\ \vec{v} = \frac{d\vec{x}}{dt}. \tag{7}$$

We consider a mesothermal plasma emission with equal electron and ion current density at the source exit, $J_{e0} = J_{i0}$. The plasma emission condition is taken to be similar to that in Ref. 6. The propellant ion is Ar. The beam ions are accelerated to 1100 eV. The temperature of the propellant plasma at the source exit is 2 eV. The simulation parameters are normalized by the electron density n_{e0} and electron temperature T_{e0} at thruster exit, the electron plasma frequency based on n_{e0}, and the Debye length based on n_{e0} and T_{e0}. Relevant plasma parameters at the thruster exit are summarized in Table 2. in both physical units and normalized values.

In order to resolve the correct ion beam neutralization and plasma expansion process, one must use the realistic ion-to-electron mass ratio so to maintain the the correct mesothermal velocity order between v_{ti}, v_{beam}, and v_{te}.[5] As the DSMC model simulates the Ar emission, the PIC simulation also uses the real ion-to-electron mass ratio for argon ions, $m_i/m_e = 40 \times 1836 = 73440$, for consistency.

In PIC simulations, macro-particles representing the beam ions and neutralizing electrons are emitted from the simulation exit into the simulation domain at each time step. The beam ions are sampled from a cold drifting Maxwellian distribution and the electrons from a stationary Maxwellian distribution. Macro-particles representing plume CEX ions are generated according to Eq. (1), from the beam ion density and neutral plume density. Macro-particles representing the ambient or the facility plasma are loaded into the simulation domain at the start of the simulation. The facility plasma density is calculated from Eq. (3). The neutral plume density $n_{n,source}$ and chamber background neutral density $n_{n,chamber}$ are obtained from DSMC.

Computationally it is not feasible to carry out a fully 3D PIC simulation using the real ion-to-electron mass ratio of Ar ions and the actual the experimental dimension in Ref. 6. In order to reduce the computational time, the 3-D PIC code is applied to simulate a 2-D configuration of the experiment with 2 cells in the y direction. Additionally, while the relative dimensions between the plasma beam radius and the vacuum chamber are kept the same as that in Ref. 6, the size of the thruster radius R_b in terms of the Debye length λ_{D0} at thruster exit is also reduced in the PIC simulation. As the purpose is to study qualitatively the effects of vacuum chamber environment on the plume potential with respect to the ambient, such an approach is sufficient because the plasma expansion outside the beam is not dependent on the beam radius as long as $R_b/\lambda_{D0} > 1$.[5]

The beam emission is along the z direction. The PIC simulation domain is the downstream region region of the thruster (with a fraction of the thruster body included), and is symmetric with respect to the $x = 0$ boundary. The boundary condition is periodic in the y direction. For in-space simulations, all other boundaries are considered to be open boundaries where the Neumann boundary condition is applied for the electric field. The absorption condition applied for the particles, and an in-flow condition corresponding to the ambient thermal flux is applied for the ambient electrons. The potential at the simulation boundary is floating for in-space simulations. For in-chamber simulations, the simulation boundary is the vacuum chamber wall where the surface potential is fixed at $\Phi = 0$ and the absorption condition is applied for all the particles.

In the simulation, the cell size is taken to be the Debye length at the source exit, λ_{D0}. The size of the beam radius at exit is taken to be $R_b = 7\lambda_{D0}$. For in-chamber simulations, the simulation domain is $163\lambda_{D0} \times 2\lambda_{D0} \times 256\lambda_{D0}$. (In the $x - z$ plane, this corresponds to approximately $23.3R_b \times 36.6R_b$.) For in-space simulations, the simulation domain needs to be sufficiently large so the plume potential is not affected by the domain boundary.[5] Different simulation domain sizes were tested. For the results shown

here, the domain for the in-space simulation is taken to be $326\lambda_{D0} \times 2\lambda_{D0} \times 512\lambda_{D0}$. (In the $x-z$ plane, this corresponds to approximately $46.6R_b \times 73.1R_b$.)

As mentioned previously, in order to establish the plume potential self-consistently in the simulation, one needs to resolve the transient process from the start of the emission. The time step resolution in the simulation is $\Delta t \times \omega_{pe} = 0.1$ ($\Delta t \times \omega_{pi} \simeq 3.7 \times 10^{-4}$), where ω_{pe} and ω_{pi} are the electron and ion plasma frequency based on the plasma density at thruster exit, respectively. Plasma-surface interaction at the chamber wall is beyond the scope of this study. Hence, for in-chamber simulations, the simulation is terminated before the ion beam front reaches the chamber wall. The simulation is run for a duration of $t\omega_{pe} = 1500$ ($t\omega_{pi} \simeq 5.5$). At the end of the simulation, the beam front is at about $\Delta z \simeq 26.2R_b$ from the thruster exit. Simulation results show that the electron-ion coupling inside the beam occurs at the electron plasma time scale while the plume plasma expansion around thruster exit completes at $t\omega_{pi} \sim 1$.[5] Hence, at the end of the simulation, the plume potential inside the beam is at the steady state.

III. Results and Discussions

III.A. Neutral Plume, Neutral Background, and Facility Plasma

Results from DSMC modeling of the neutrals are shown in Figs. 2 through 4. Fig. 2 shows the density contours for the neutral plume emitted from the thruster, $n_{n,source}$. The neutral plume is the only neutral environment when the thruster operates in-space. The density distribution corresponds to that of a classical thermal diffusion. When the thruster operates inside a vacuum chamber, the neutral density distribution will be affected by the vacuum chamber wall and the pumping speed. Fig. 3 shows the neutral environment under the in-chamber condition. Fig. 4 further shows the density profile along the thruster axis for the total neutral density as well as the densities associated with the neutral plume, the neutrals reflected from the side wall, and the neutrals reflected from the gate valve.

The results show that the neutral density distribution close to the thruster exit is dominated by the molecules emitted from the thruster. However, for the operating conditions considered, the total Ar number density in the vacuum chamber starts to deviate significantly from that of the thruster generated neutral plume at $z \sim 3R_b$ due to molecules reflected from the chamber wall and the gate valve. In Fig. 4, the background neutral density in the chamber asymptotes for $z/R_b > 10$ at about $n_{n,chamber} \sim 2 \times 10^{17}\text{m}^{-3}$. For comparison, the density associated with the neutral plume emitted from the thruster is about $n_{n,source} \sim 2 \times 10^{16}$ m^{-3} at $z/R_b \sim 25$. Hence, the neutral environment in a vacuum chamber is very different from the neutral plume under in-space condition. The pressure inside the vacuum chamber is quite uniform due to neutral molecule reflections at the chamber wall. In Ref. 6, a pressure probe was located at the chamber wall at a downstream distance of $z/R_b \sim 8$. The probe measured a background pressure of 3.8×10^{-6} Torr ($\approx 5 \times 10^{-4}$ Pa). The pressure obtained from the DSMC simulation at that location agrees well with the measured value in Ref. 6.

The neutral background in a vacuum chamber leads to the generation of the facility plasma. The facility plasma consider here is dominated by CEX production in the chamber. The number of CEX ions produced between the ion beam and the neutral background is given by $\int \dot{n}_{cex,chamber}(\vec{x})dV$, where $\dot{n}_{cex,chamber}(\vec{x})$ is given by Eq. (3) and the integral is over the beam volume. As these CEX ions propagate radially outward from the beam at approximately the ion acoustic velocity C_s, the facility plasma density far away from the thruster at steady state is

$$n_{facility} \simeq \frac{\int \dot{n}_{cex,chamber}(\vec{x})dV}{C_s \cdot A}. \tag{8}$$

where A is the surface area of the beam.

The PIC simulation was run using the real ion to electron mass ratio for Ar for a simulation duration of $t\omega_{pi} \simeq 5.5$. If one would generate the CEX ions as the beam ions propagate through the domain, the simulation time would be too short to establish a steady state facility plasma in the domain because the CEX ions move at a much slower speed than that the beam ions. Hence, in the simulation, the steady state facility plasma is loaded at the beginning of the simulation with a density calculated from Eq. (8). For the experimental conditions considered in this paper, we find that the facility plasma density in the chamber to be $n_{chamber}/n_{e0} \simeq 5 \times 10^{-3}$.

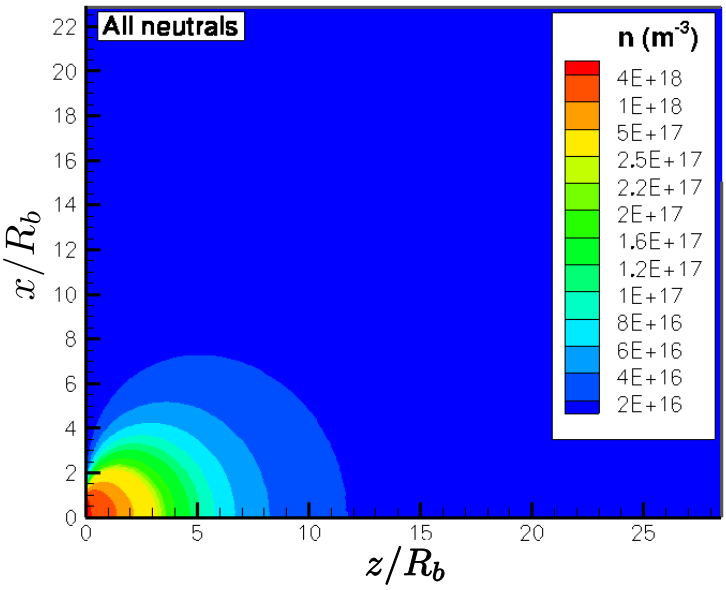

Figure 2. DSMC simulations of neutrals emitted from source under in-space condition: Neutral plume density contours

III.B. Plasma Plume Potential

The plasma plume potential is compared for three different background plasma environments. In Case 1, a mesothermal beam is emitted into an ambient space plasma. The ambient plasma density is taken to be similar to the typical solar wind plasma density, $n_{ambient} \sim 1.5 \times 10^6$ m^{-3}. Hence, $n_{ambient}/n_{e0} \simeq 10^{-9}$. In Case 2, a mesothermal beam is emitted into a vacuum chamber. The facility plasma density is taken to be the value calculated in the last section, $n_{chamber}/n_{e0} \simeq 5 \times 10^{-3}$. In Case 3, we reduce the facility plasma density to be the same as the $n_{ambient}$ in Case 1 for comparison, $n_{chamber}/n_{e0} \simeq 10^{-9}$.

Figure 5 shows the density contours for the beam ions, neutralizing electrons, and propellant CEX ions for Case 2 at $t\omega_{pe} \simeq 1500$ ($t\omega_{pi} \simeq 5.5$). The beam ions and neutralizing electrons have formed a neutralized, steady state beam behind the beam front. The electron-ion coupling process was discussed in detail in Ref. 5. At $t\omega_{pi} \simeq 5.5$, the CEX ions generated in the simulation have not propagated very far from the beam. (The plume CEX density contours shown in Fig. 5c are still within about $\sim 5.5R_b$ downstream of the thruster exit.) Hence, Fig. 5c shows the early time plume CEX ion density distribution. However, since $n_{cex,source}$ is orders of magnitude less than the beam plasma density, the plume potential is not expected to be affected significantly by including only the early time plume CEX ions. The density contours for Case 1 and Case 3 are similar to that shown in Fig. 5. This is to be expected. As the $n_{ambient}$ or $n_{chamber}$ is orders of magnitude smaller than the beam density, the presence of a background plasma does not have a noticeable effect on the plume density profile.

Figure 6 shows the potential contours for the three cases. Figure 7 compares 1-D potential profiles Φ vs. x (the transverse direction to beam direction) at three downstream distances from thruster exit. The beam potentials shown are already at the steady state. For comparison with Case 2 and 3, the ambient potential in Case 1 is shifted to $\Phi = 0$ in these plots.

The results show that the potential profiles for all three cases are similar within the core region of the beam but different in the region outside the beam. The deviation starts at around $x > 3R_b$. In particular, in Case 2, a potential plateau shows up in the region approximately $5R_b < x < 20R_b$ before Φ decreases further to $\Phi = 0$ at the chamber surface ($x \simeq 23.3R_b$). A sheath is also evident near the chamber wall. These features are due to the presence of the facility plasma. The facility plasma terminates the beam expansion when the propellant plasma density becomes smaller than $n_{chamber}$. Even though the facility plasma density in Case 2 is about 3 orders of magnitude smaller than the propellant plasma density at thruster exit ($n_{chamber}/n_{eo} \sim 5 \times 10^{-3}$, $n_{chamber}/n_{io} \sim 1.5 \times 10^{-3}$), its effect in reducing the potential difference between the beam center and the background is significant. In all the cases, the potential at beam center is $\Phi_0 \simeq 7.5$. In Case 2, the potential plateau outside the beam is $\Phi_{chamber} \simeq 2.1$. Hence, the potential

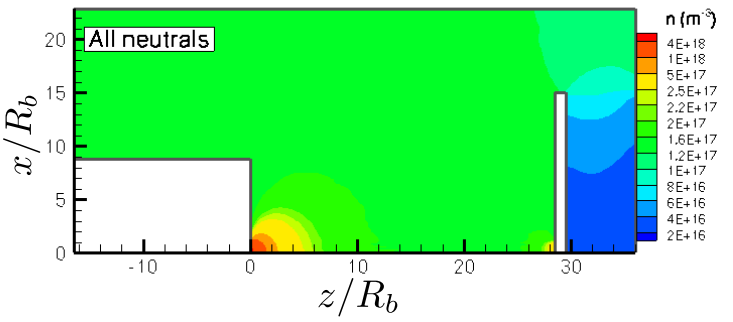

(a) Total neutral density contours

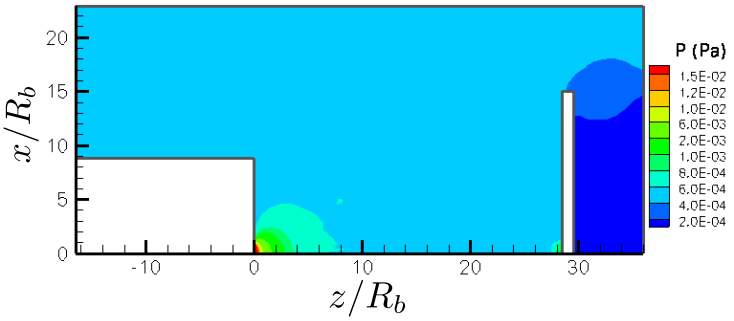

(b) Neutral pressure contours

Figure 3. DSMC simulations of neutrals for in-chamber testing of a plasma source: Total neutral density contours in vacuum chamber

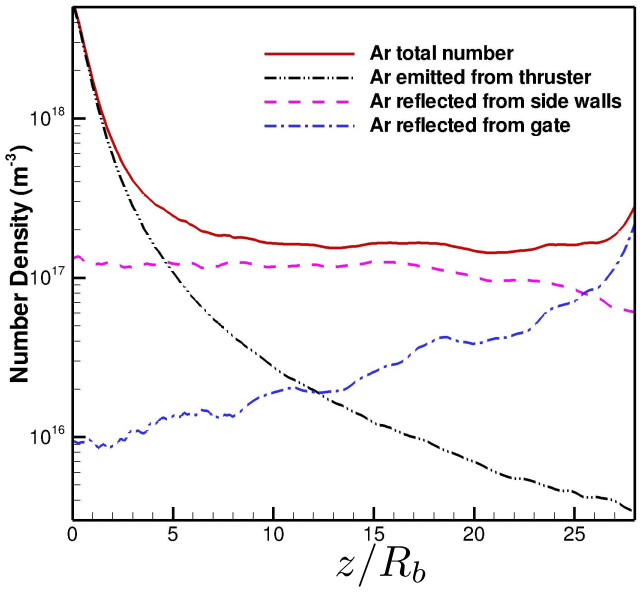

Figure 4. Density profile of each neutral population in vacuum chamber along the thruster axis

difference between the beam center and the facility plasma in Case 2 is about $\Delta\Phi \simeq 5.4$. Comparing to Case 1, this represents approximately a reduction of 28% in beam potential with respect to the background.

If we reduce the facility plasma density to that of the typical solar wind density as in Case 3, the

potential plateau disappears. However, in this case, the plasma expansion outside the beam is terminated by the boundary condition of $\Phi = 0$ at the chamber wall. Due to the smaller space available for plasma expansion, the plume potential outside the beam decreases more quickly than that in Case 1. Hence, the beam potential is still affected by the vacuum chamber.

IV. Summary and Conclusions

DSMC and PIC simulations are applied to study the potential of a mesothermal plasma plume in a vacuum chamber. The results show that the beam potential with respect to the ambient in a vacuum chamber may be significantly different from that in a space plasma environment. This is because the facility plasma in a vacuum chamber can terminate the plume expansion process and thus reduce the beam potential. This simulation study considers the vacuum chamber experiment in Ref. 6. For this particular experiment, the facility plasma density is found to be about 3 orders of magnitude smaller than the beam plasma density at source exit. The simulation results show that the contribution from a facility plasma similar to that in Ref. 6 can lead to approximately a reduction of 28% in beam potential with respect to the ambient. This suggest that the plume potential measured in a vacuum chamber may be significantly lower than that under the in-space condition. Most existing plume models are based on a hybrid PIC approach which require the plume potential to be provided as an input parameter. Since predictions of the plume potential are mostly based on vacuum chamber measurements, an under prediction of the plume potential will result in under estimation of plume interaction effects such as the backflow of CEX ions and ionized contaminants in subsequent plume modeling studies.

In order to establish the beam potential self-consistently, PIC simulations need to resolve the transient process from the start of the beam emission. In this paper, the simulation time is not long enough to include the effect from the steady state plume CEX plasma on the beam potential. Hence, the reduction of the beam potential observed in the simulation here represents only the lower bound reduction in a vacuum chamber. This study only considered one particularly vacuum chamber experiment. A future study will address the effects from the plume CEX plasma and different vacuum chamber environments.

Acknowledgments

We would like to thank the USC Center for High-Performance Computing and Communications (HPCC) for computing resources. D. Han would also like to thank USC graduate school endowed fellowship for travel grant to IEPC. This work is supported by NASA grant NNX11AH21G.

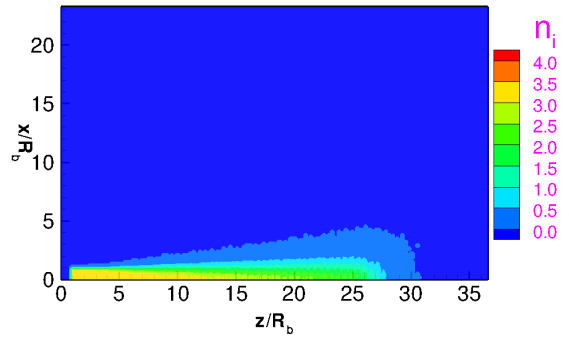

(a) Beam ions

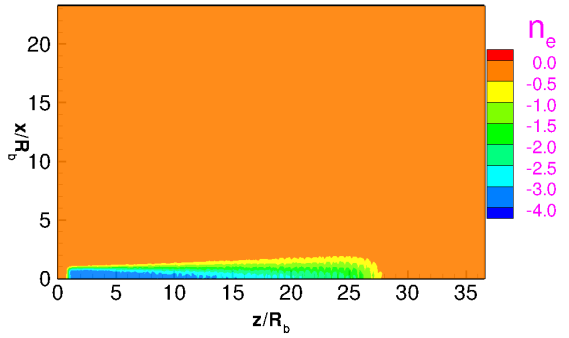

(b) Neutralizing electrons

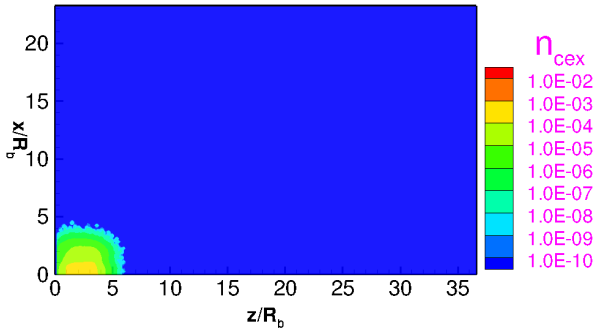

(c) Plume CEX ions

Figure 5. Density contours for beam ions, neutralizing electrons, plume CEX ions for Case 2

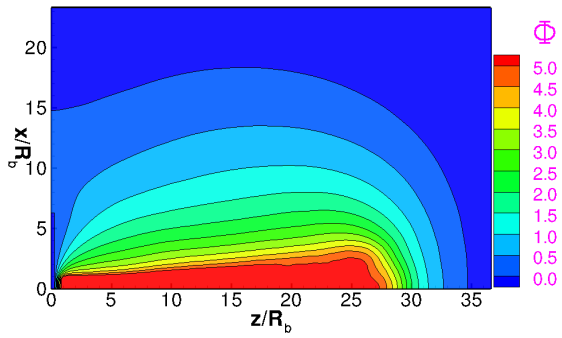

(a) Case 1

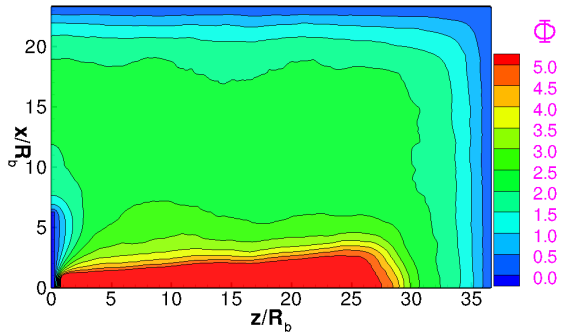

(b) Case 2

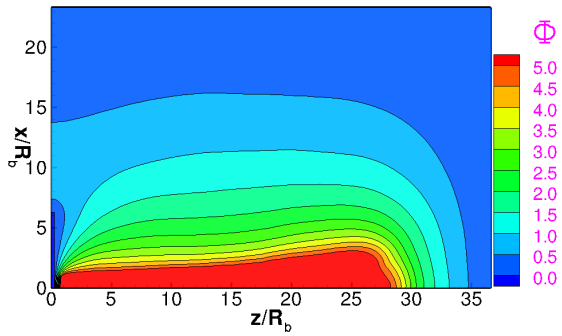

(c) Case 3

Figure 6. Potential contours for Case 1 (in-space), Case 2 (in-chamber), and Case 3 (in-chamber with an artificial facility plasma density)

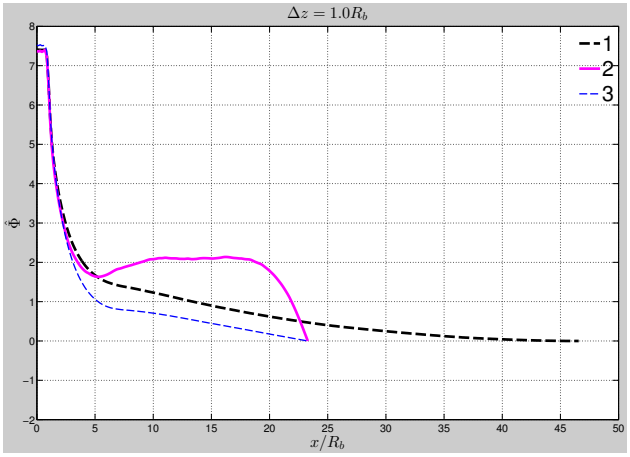

(a) $\Delta z = 1.0R_b$

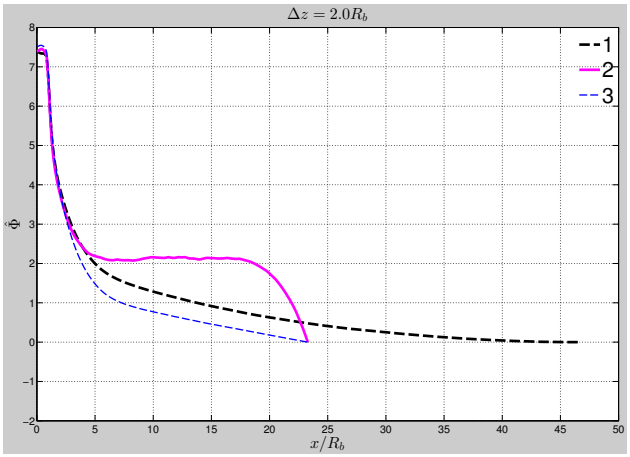

(b) $\Delta z = 2.0R_b$

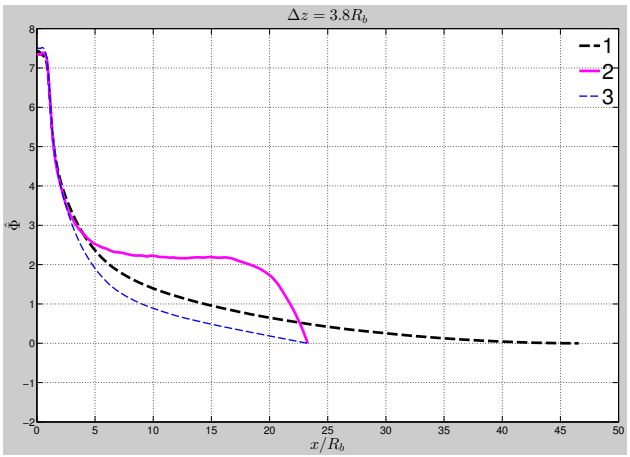

(c) $\Delta z = 3.8R_b$

Figure 7. Comparison of 1-D potential profiles at several downstream locations from thruster exit between Case 1, Case 2, and Case 3.

References

[1]J. Wang, D. Brinza, D. Young, J. Nordholt, J. Polk, M. Henry, R. Goldstein, J. Hanley, D. Lawrence, and M. Shappirio, "Deep Space One Investigations of Ion Propulsion Plasma Environment", *J. Spacecraft and Rockets*, 2000, 37(5), pp545-555.

[2]J. Wang, D. Brinza, and M. Young, "Three-Dimensional Particle Simulations of Ion Propulsion Plasma Environment for Deep Space 1", *J. Spacecraft and Rockets*, 2001, 38(3), pp433-440.

[3]D. Brinza, J. Wang, J. Polk, and M. Henry, "Deep Space 1 Measurements of Ion Propulsion", *J. Spacecraft and Rockets*, 2001, 38(3), pp426-432.

[4]J. Wang, Y. Cao, R. Kafafy, J. Pierru, and V. K. Decyk, "Simulations of Ion Thruster Plume-Spacecraft Interactions on Parallel Supercomputer", *IEEE Trans. Plasma Sciences*, 2006, 34, pp2148-2158.

[5]J. Wang, O. Chang, and Y. Cao, "Electron-Ion Coupling in Mesothermal Plasma Beam Emissionl", *IEEE Trans. Plasma Sciences*, 2012, 40, pp230-236.

[6]J. Polansky, J. Wang, and N. Ding, "Experimental Investigation on Plasma Plume Potential", *IEEE Trans. Plasma Sciences*, 2013, 41, pp3438-3447.

[7]O. Buneman and G. Kooyers, "Computer Simulation of the Electron Mixing Mechanism in Ion Propulsion", *AIAA J.*, 1963, 1(11), pp2525-2528.

[8]R. Wadhwa, O. Buneman, and D. Brauch, "Two-Dimensional Computer Experiments on Ion Beam Neutralization", *AIAA J.*, 1965, 3(6), pp1076-1081.

[9]D. Dunn and T. Ho, "Longitudinal Instabilities in an Electrostatic Propulsion Beam with Injected Current Neutrality", *AIAA Preprint 63041*, 1965.

[10]H. Derfler, "Nonexistence of Quiescent Plasma States in Ion Propulsion", *Physics of Fluids*, 1964, 7(10), pp1625-1637.

[11]A. Wheelock, D. Cooke, and N. Gatsonis, "Ion Beam Neutralization Processes for Electric Micropropulsion Applications", AIAA/ASME/SAE/ASEE Joint Propulsion Conf., Huntsville, AL, 2003, Paper AIAA 2003-5148.

[12]L. Brieda and J. Wang, "Modeling Ion Thruster Beam Neutralization Using a Fully Kinetic ES-PIC Code", AIAA/ASME/SAE/ASEE Joint Propulsion Conf., Tucson, AZ, 2005, Paper AIAA 2005-4045.

[13]J. Wang and Y. Cao "Modeling Ion Beam Neutralization", Int. Electric Propulsion Conf., Florence, Italy, 2007, Paper IEPC 2007-241.

[14]J. Wang and H. Usui, "Kinetic Simulations of Ion Beam Neutralization", Int. Electric Propulsion Conf., Ann Arbor, MI, 2009, Paper IEPC 2009-263.

[15]J. Polansky, "Laboratory Investigations of the Near Surface Plasma Field and Charging at the Lunar Terminator", Ph.D Dissertation, University of Southern California, 2013.

[16]G. A. Bird, *Molecular Gas Dynamics and the Direct Simulation of Gas Flows*, Oxford University Press, 1994

[17]Y. Hu, S. Chen, and Q. Sun "Hypersonic Aerodynamics of a Flat Plate: Bridging Formula and Wall Temperature Effects", *AIP Conference Proceedings*, 2012, 1501, pp1493-1499.